Journal of Materials Chemistry C

An approach towards plastic scintillators from thermally activated delayed fluorescent dyes and cross-linkable bismuth compounds

Journal:	*Journal of Materials Chemistry C*
Manuscript ID	TC-ART-09-2022-004165.R1
Article Type:	Paper
Date Submitted by the Author:	31-Oct-2022
Complete List of Authors:	Abraham, Silja; Georgia Institute of Technology, School of Chemistry and Biochemistry Fuentes-Hernandez, Canek; Georgia Institute of Technology, School of Electrical and Computer Engineering; Northeastern University College of Engineering, Department of Electrical and Computer Engineering Mukhopadhyay, Sharmistha; Georgia Institute of Technology, Nuclear and Radiological Engineering Singh, Kumar; Georgia Tech Research Institute, Advanced Concepts Laboratory Kim, Hyung Nun; Georgia Institute of Technology, Woodruff School of Mechanical Engineering Moreno, Oliver; Georgia Institute of Technology, School of Electrical and Computer Engineering Tran, Claire; Georgia Institute of Technology, Woodruff School of Mechanical Engineering Kumar, Dharam; Georgia Institute of Technology, School of Chemical & Biomolecular Engineering Stooksbury, John; Georgia Institute of Technology, Nuclear and Radiological Engineering Kalidindi, Surya; Georgia Institute of Technology, School of Materials Science and Engineering Hertel, Nolan; Georgia Institute of Technology, Nuclear and Radiological Engineering Shannon, Michael; Georgia Tech Research Institute, Advanced Concepts Laboratory Kippelen, Bernard; Georgia Institute of Technology College of Engineering, School of ECE

An approach towards plastic scintillators from thermally activated delayed fluorescent dyes and cross-linkable bismuth compounds

Silja Abraham[1], Canek Fuentes-Hernandez[1,2], Sharmistha Mukhopadhyay[3], Kumar Singh[4], Hyung Nun Kim[5], Oliver Moreno[1], Claire M. Tran[5], Dharam Raj Kumar[6], John C. Stooksbury[3], Surya R. Kalidindi[5], Nolan E. Hertel[3], Michel P. Shannon[4], and Bernard Kippelen[1*]

1. Center for Organic Photonics and Electronics (COPE), School of Electrical and Computer Engineering, Georgia Institute of Technology, Atlanta, GA-30332, United States.
2. Current address: Department of Electrical and Computer Engineering, Northeastern University, Boston MA-02115, United States.
3. Nuclear and Radiological Engineering, Georgia Institute of Technology, Atlanta, GA-30332, United States.
4. Advanced Concepts Laboratory, Georgia Tech Research Institute, Atlanta, GA-30332, United States.
5. Woodruff School of Mechanical Engineering, Georgia Institute of Technology, Atlanta, GA-30332, United States.
6. School of Chemical & Biomolecular Engineering, Georgia Institute of Technology, Atlanta, GA-30332, United States.

[*]Corresponding author: kippelen@gatech.edu

Keywords: organic scintillators, gamma spectroscopy, bismuth compound, TADF

Abstract

Cross-linked polyvinyltoluene (PVT) based plastic scintillators loaded with dyes exhibiting thermally activated delayed fluorescence (TADF) and various amounts of (caproate)di-(methacrylate) bismuth (CMB) were developed. The co-polymerization of vinyl toluene monomer loaded with different weight ratios of CMB and 1 wt. % of TADF dye yielded highly transparent cross-linked plastic scintillators with intense green photoluminescence. The thermal and mechanical properties of the scintillators were investigated using thermogravimetric analysis (TGA), differential scanning calorimetry (DSC) and micro indentation techniques. Their performance for radiation detection was assessed by performing gamma spectroscopy using a Cs-137 source and benchmarked to commercial plastic scintillators. The loading of CMB was guided by Monte Carlo N-Particle (MCNP) simulations. The results of this study show that the cross-linking approach and the use of TADF dyes yield scintillators with good mechanical properties with a uniaxial yield strength up to ~ 66 MPa for compositions loaded with 40 wt.% of CMB and high optical quality. However, the light yield in gamma spectroscopy experiments is found to be reduced with the addition of CMB, suggesting a trade-off between mechanical yield strength and light yield in gamma spectroscopy.

Introduction

Robust, low-cost, high-performance organic scintillators with spectroscopic capabilities could enable their seamless integration in unmanned vehicle (UxV) systems (e.g. as structural components) and in other portable sensor systems relevant for countering nuclear threats.[1, 2] In particular, plastic scintillators are of interest due to their mechanical properties and their potential to be fabricated at low cost into objects of various shapes using injection molding or other additive manufacturing techniques.[3] This rapid and responsive capability will make them highly suitable for easy incorporation into an array of platforms including manportable, manwearable and unmanned systems for radiological and nuclear search to counter nuclear threats.

Plastic scintillator detectors are comprised of a polymer matrix loaded with photoluminescent organic dyes and in some cases with organic or inorganic compounds containing heavy elements to increase the probability of interaction between the scintillator and ionizing radiation of interest, herein gamma rays. The interaction between a gamma ray and a plastic scintillator yields energetic electrons, produced via the photoelectric effect or Compton scattering, that lead to the formation of singlet and triplet excited states, i.e. excitons, with a ratio of 1:3 according to spin statistics. When the light-emitting organic compounds in a plastic scintillator consist of fluorescent dyes, the radiative recombination of triplet excitons is spin-forbidden and 75% of the excitons do not contribute to light emission due to non-radiative recombination. To overcome the loss of triplet excitons two strategies exist: the use of phosphorescent dyes or dyes that exhibit thermally activated delayed fluorescence (TADF).[4-7] While both of these strategies have the potential to yield scintillators with 100% luminescence quantum yield (LQY) in gamma spectroscopy, they also yield a slower photoluminescence than those of conventional fluorescent dyes, with characteristic times in the microsecond

range. In these so-called TADF dyes, a small energy gap between singlet and triplet excited states enables efficient reverse intersystem crossing (RISC) at room temperature and LQY values that can approach 100% and are consequently attractive to increase the light yield of plastic scintillators.[8-11]

To date reports on the use of TADF dyes in plastic scintillators with a polyvinyltoluene (PVT) polymer matrix remain scarce.[9, 10] In these studies, PVT scintillators loaded with TADF dyes such as 9-(4-3-[4-(3,6-dioctyl-9H-carbazol-9-yl)benzene-sulfonyl]benzene-sulfonyl phenyl)-3,6-dioctyl-9H-carbazole (DOC-mBPSB at 10 wt.%) and 9-(4-4-[4-(3,6-Dioctyl-9H-carbazol-9-yl)benzenesulfonyl]benzenesulfonyl phenyl)-3,6-dioctyl-9H-carbazo le (DOC-pBPSB at 10 wt.%)[10] or 9-(4-(4,6-diphenyl-1,3,5-triazin-2-yl)-2-methylphenyl)-3,6-dioctyl-9H-carbazole (OCz-TRZ at 30 wt.%)[9] where found to have limited solubility which prevented the use of higher loading ratios suitable for pulse shape discrimination (PSD) (for PSD, higher loading of fluorophores is required). In addition, none of these scintillators was loaded with compounds containing heavy elements with high atomic numbers (Z) such as bismuth (Bi), preventing the observation of a photopeak during detection of gamma radiation through the photoelectric effect.

Plastic scintillators have been loaded with compounds containing high-Z elements using quantum dots, scintillation nanocrystals, and high-Z organometallic compounds to increase the γ-stopping power and photoelectric cross-section.[3, 12] Among them scintillators with standard fluorophores (fluorescent dyes) and bismuth compounds such as triphenylbismuth and bismuth carboxylates showed better gamma stopping power. Samples of PVT based scintillators (6.5 in^3) with 20 wt.% Bi-pivalate were investigated by gamma ray spectroscopy (~1 MeV) and showed photopeaks with 13% energy resolution at 662 keV.[13-16]

In all these cases, addition of bismuth seems to be quenching the light yield due to heavy atom effects.[13, 14] So the main challenge is to incorporate the bismuth without largely affecting the light yield. To improve the light yield, a phosphorescent dye bis[2-(4,6-difluorophenyl)pyridinato-C 2 ,N](picolinato)iridium(III) was used as a secondary emitter (a secondary wave length shifter used along with a primary dye to mitigate self-absorption of primary dye by absorbing the photons emitted by primary dye and re-emit at longer wavelength) in poly(9-vinylcarbazole) matrix along with triphenyl bismuth. This material combination achieved both singlet and triplet exciton harvesting and thereby high light yield (~30,000 photons/MeV) compared to the scintillator with same bismuth composition with a standard fluorophore diphenylanthracene (~12,000 photons/MeV).[17]

Here, we report on the properties of vinyl toluene plastic scintillators loaded with a methacrylate linked (caproate)di-(methacrylate) bismuth (CMB) high-Z material and with 4CzIPN or tBuCzDBA, green emitting TADF dyes.[6, 14, 18] In these scintillators, CMB can undergo cross-linking with vinyl toluene matrix to form thermally and mechanically stable plastic scintillators. This paper gives new insights on bismuth loaded scintillators with TADF dyes by comparing their light yields, effect of addition of bismuth on their optical, thermal and mechanical properties, Monte Carlo N-Particle (MCNP) simulations to understand the response of these plastic scintillators with bismuth loading and gamma ray spectroscopy.

Experimental

Materials and Methods

Methylstyrene (vinyltoluene) (96%), divinyl benzene, 2,2′-Azobis(2-methylpropionitrile) (AIBN) (99%), hexanoic acid (99%) were purchased from Sigma-Aldrich. Triphenyl bismuth (98+%) was purchased from Alfa Aesar, and further purified by recrystallization from chloroform-methanol solution and dried in vacuum.

2,4,5,6-Tetra(9H-carbazol-9-yl)isophthalonitrile (**4CzIPN**), and 5,10-Bis(4-(3,6-di-tert-butyl-9H-carbazol-9-yl)-2,6-dimethylphenyl)-5,10-dihydroboranthrene (**tBuCzDBA)** were purchased from Lumtec Corp. (Caproate)di-(methacrylate) bismuth **(CMB)** was synthesized from triphenyl bismuth and hexanoic acid following the procedure reported elsewhere (**Figure S1**).[14] ^{1}H and ^{13}C NMR spectra were recorded on a Bruker AV3 HD 500 MHz NMR spectrometer and the resulting ^{1}H NMR spectra was the sum of 32 transients.

Synthesis of (caproate)di-(methacrylate) bismuth (CMB)

Triphenylbismuth (2g, 4.542 mmol), methacrylic acid (0.782 g, 9.084 mmol) and hexanoic acid (0.528 g, 4.542 mmol) were sealed inside a 30 mL glass bottle. The mixture was heated to 85 ^{o}C and then vigorously stirred at 85 ^{o}C for 2h. Then the resulting mixture was cooled down to room temperature. The side product, benzene was evaporated under reduced pressure.

^{1}H NMR: (700 MHz, DMSO-D_6) δ: 5.89 (s, 2H), 5.48 (s, 2H), 2.07 (t, J = 7 Hz, 2H), 1.81 (s, 6H), 1.50 (m, 2H), 1.26 (m, 4H), 0.85 (t, J = 7 Hz, 3H).

^{13}C NMR: (700 MHz, DMSO-D_6) δ: 181.11, 174.31, 141.74, 124.52, 38.05, 31.33, 25.09, 22.41, 18.88, 14.33.

Scintillator fabrication

Vinyltoluene (monomer) and divinylbenzene (cross-linker) were passed through an inhibitor removal column to remove the inhibitors. 1 wt.% of TADF fluorophore **4CzIPN/tBuCzDBA** was dissolved in required amount of vinyltoluene and divinylbenzene. For high Z bismuth loaded scintillators, appropriate amounts of **CMB** (5-40 wt.%) was used along with 1 wt.% fluorophore. The mixture was degassed by applying vacuum and nitrogen. 0.5 wt.% of AIBN initiator was then added, and the mixture was poured into a silane-treated glass mold. These molds were kept at 85 ^{o}C for 1.5 days for complete curing. For the cross-linker free sample **AR0** (1 wt.% **4CzIPN**,

99 wt.% Vinyl toluene), the curing time is 5 days at 85 °C. The scintillators were cooled to room temperature and then demolded. Finally, the scintillators were polished.

UV–vis spectra were measured using a Cary 5000 UV–Vis–NIR spectrophotometer.

Fluorescence and transient photoluminescence were recorded on a Jobin Yvon Fluorolog-3 spectrofluorimeter equipped with a photomultiplier tube (Horiba R928), pulsed xenon lamp, and pulsed LED excitation source (NanoLED). Fluorescent lifetime analysis was done using DAS6 decay analysis software.

TGA and DSC analysis were done using Netzsch STA-409 Luxx– thermogravimetric analyzer – differential scanning calorimeter (TGA-DSC). The temperature program used for all these experiments was from 25 – 900 °C at 10 °C/min under the flow of nitrogen.

Mechanical Properties

Spherical micro-indentation was used to measure mechanical properties of the different specimen, which were approximately 7 mm in thickness. The spherical indenter tip was 6.35 mm in radius, and the sample was loaded up to 100 N. Care was taken not to load the samples to the point where the underlying substrate influenced the measurements. This is because the stress and strain fields under the indenter extend far beyond the primary indentation deformation zone. Using spherical indentation stress-strain analysis protocols[19, 20], one can convert the raw load-displacement measurements into indentation stress-strain curves as shown in Figure S3b. Using the indentation stress-strain curve, one can determine the Young's modulus and the indentation yield strength at 0.2% offset indentation plastic strain. Furthermore, a relationship between the indentation yield strength (Y_{ISS}) and uniaxial yield strength (Y_{USS}) was established to be $\left(\frac{Y_{ISS}}{2} = Y_{USS}\right)$ in prior studies using FEM simulations for a wide range of material classes including polymeric materials [21-24]. This relationship was used in this work to

estimate uniaxial yield strengths from the extracted indentation yield strengths.

Gamma spectroscopy

Scintillators were wrapped in a Teflon (PTFE) tape and mounted onto Hamamatsu R2059 photomultiplier tubes (PMT) using silicone optical grease. The signals from the PMT output were connected to an ORTEC 133 preamplifier and 1 μs second shaping time was used in ORTEC 571 shaping amplifier before the signals were recorded with MCB multichannel analyzer.

The aim of our measurement was to compare the Compton edge pulse heights with commercially available Eljen Technology, EJ 200 cylindrical scintillator of diameter 1.25 cm and 1.5 cm length and under identical experimental condition. PMT was biased to -2700V, Cs-137 source (0.49 μCi on Dec 9, 2005) was used at distance of 3.175 cm from the scintillator for 3600 s for the measurements. The experimental setup is shown in Figure S7.

Results & discussion

Scintillator Fabrication

Cross-linked PVT plastic scintillators were loaded with either the cross-linkable high-Z material – CMB, at concentrations between 5 and 40 wt.%, or with the cross-linker DVB, at a concentration of 4.5 wt.%, and the TADF dyes - 4CzIPN, or tBuCzDBA at a concentration of 1 wt.%. Figure 1 shows the chemical structure of all materials used. Samples containing 4CzIPN are referred to as samples AX, where X stands for the value of the wt.% concentration of CMB. Similarly, samples containing tBuCzDBA are referred to as samples BX. Table 1 and 2 show the composition and density of all scintillators. In samples A40 and B40, a maximum elemental bismuth concentration of 17 wt.% was achieved. The co-polymerization of vinyl toluene with either with DVB or CMB resulted in highly transparent cross-linked polymers and scintillators with good

optical clarity (Figure 2a &2d).

The green-emitting TADF dyes 4CzIPN and tBuCzDBA were chosen because of their small single to triplet energy gap (ΔE_{ST}) of 83 meV and 22 meV, respectively, their high PLQY (86 % for thin film of tBuCzDBA 10% doped in 4,4'-Bis(N-carbazolyl)-1,1'-biphenyl, (CBP), and 94 ± 2% for 4CzIPN in toluene at a concentration of 10^{-5} mol l^{-1}) and relatively short excited-state lifetime of delayed emission of τ_d = 5.1 μs (in toluene) for 4CzIPN and of τ_d = 2.1 μs (10% doped in 4,4'-Bis(N-carbazolyl)-1,1'-biphenyl, CBP) for tBuCzDBA.[6, 18] CMB was synthesized from triphenyl bismuth and hexanoic acid following the procedure reported elsewhere and analyzed using ^{1}H and ^{13}C NMR (Scheme S1 & Figure S1).[14]

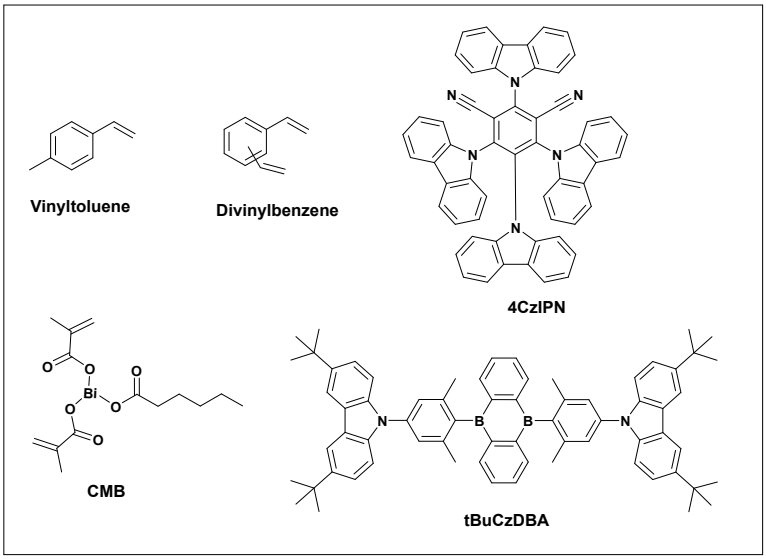

Figure 1. Chemical structures of vinyltoluene (monomer), divinylbenzene (cross-linker), (caproate)di-(methacrylate) bismuth (CMB), and TADF materials- 4CzIPN, and tBuCzDBA.

Table 1. The composition, density, and mechanical properties of 4CzIPN loaded scintillators with 0, 5, 10, 40 wt.% of CMB.

PVT Scintillator	Vinyl toluene (wt.%)	DVB (wt.%)	4CzIPN (wt.%)	CMB (wt.%)	Bismuth (wt.%)	Density (g/cm^3)	Young's Modulus (GPa)	Uniaxial Yield strength (MPa)
AR0	99	0	1	0	0	-	2.87± 0.18	~40
A0	94.05	4.95	1	0	0	1.019	2.62 ± 0.03	~51
A5	94	0	1	5	2.11	1.055	-	-
A10	89	0	1	10	4.23	1.092	-	-
A40	59	0	1	40	16.91	1.267	2.72 ± 0.04	~66

Table 2. The composition and density of tBuCzDBA loaded scintillators with 0, 5, 10, 40 wt.% of CMB.

PVT Scintillator	Vinyl toluene (wt.%)	DVB (wt.%)	tBuCzDBA (wt.%)	CMB (wt.%)	Bismuth (wt.%)	Density (g/cm^3)
B0	94.05	4.95	1	0	0	1.035
B5	94	0	1	5	2.11	1.064
B10	89	0	1	10	4.23	1.088
B40	59	0	1	40	16.91	1.259

Optical and thermo-mechanical properties

The optical, thermal and mechanical properties were compared for the compositions with no CMB content and with 40 wt.% of CMB. Figure 2a and 2b show the absorption spectra and photoluminescence spectra of compositions A0 and A40. The absorption spectra of A0 and A40 extend into the visible spectral region up to ca. 470 nm. The photoluminescence spectra of A0 and A40 (with a 440 nm excitation wavelength to excite 4CzIPN) is shown in Figure 2b. Both samples show intense green photoluminescence (corresponding to the emission 4CzIPN), but the photoluminescence intensity of A40 is found to be lower (*ca.* 12 %) than that of the A0 scintillator. Figure 2c & S2a show the temporal evolution of the photoluminescence. Lifetime analysis of these data yields a prompt lifetime (τ_p) and delayed lifetime (τ_d) of 12.2 ns and 3.3 μs, respectively, for A0, and 12.7 ns and 3 μs, respectively, for A40.

These results show that the addition of Bi does not significantly affect the excited-state lifetime.

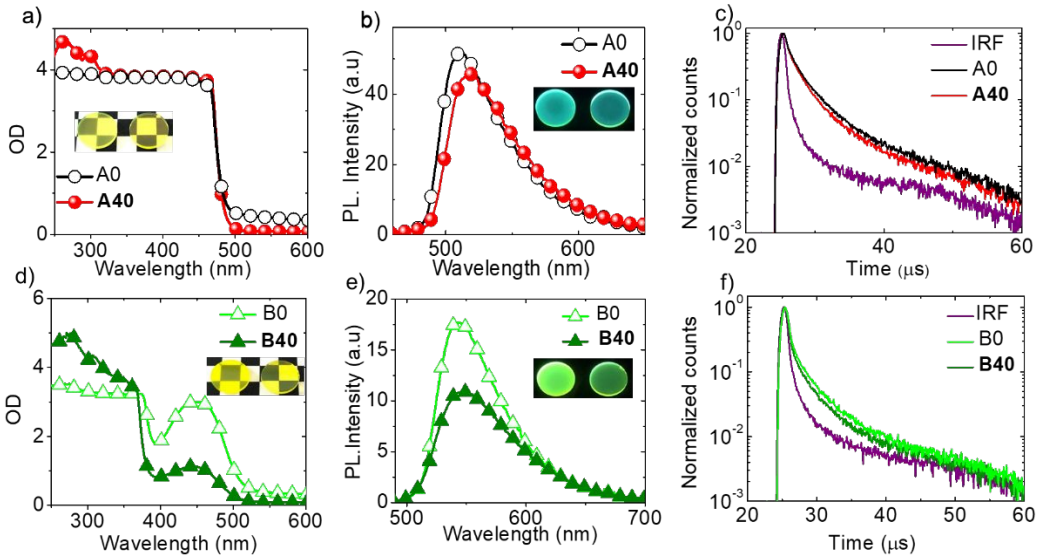

Figure 2. Absorption spectra of a) A0 (2.90 mm) and A40 (2.71 mm), d) B0 (2.57 mm) and B40 (2.74 mm) (Inset show the images of samples under room light); Photoluminescence spectra of b) A0 and A40, e) B0 and B40 (λ_{ex} = 440 nm) (Inset show the images of samples under UV light (365 nm)); Delayed lifetime traces of c) A0 and A40, f) B0 and B40.

Figure 2d shows the absorption spectra of compositions B0 and B40, which extend to 520 nm. Figure 2e shows their photoluminescence spectra with a 440 nm excitation wavelength (where excitation occurs mainly in tBuCzDBA). Both samples show intense green fluorescence, while a decrease in photoluminescence intensity (*ca*. 39 %) is observed in sample B40 compared to sample B0. The lifetime analysis of samples B0 and B40 shows a prompt lifetime (τ_p) and delayed lifetime (τ_d) of 40.7 ns and 2.9 μs, respectively, for B0, and 61.2 ns and 2.6 μs, respectively, for B40 (Figure 2f & S2b).

The mechanical properties of samples A0 and A40 containing a cross-linker and sample AR0 without cross-linker were investigated using the micro-indentation technique. Indentation-based techniques were selected because the available material

did not permit standard tests requiring a so-called dog-bone specimen. The indentation-based protocols require minimal sample preparation, which essentially involves producing a flat and polished surface. The micro-indentation test set-up and the details of the test and analysis protocols used in this study are based on recent prior work.[19, 20] These methods utilize a spherical indenter tip, and are largely based on Hertz's theory.[19, 20] A salient feature of these protocols is that they produce an indentation stress-strain response reflecting the intrinsic material response from the raw indentation load-displacement measurements. These protocols provide estimates of the sample's Young's modulus and uniaxial yield strength (estimated as indentation yield strength divided by 2.0).[21-24]

Figure 3a shows the indentation stress-strain curves measured on samples A0 and A40. The Young's modulus and uniaxial yield strength for AR0 (PVT matrix without any cross-linking) were estimated (Figure S3) to be 2.9 ± 0.2 GPa and 40.4 ± 1.4 MPa, respectively, while the A0 (cross-linked PVT matrix with divinylbenzene) sample exhibited Young's modulus and uniaxial yield strength of 2.62 ± 0.03 GPa and approximately ~51 MPa, respectively. Sample A40 shows a modulus of 2.72 ± 0.04 GPa and uniaxial yield strength of approximately ~66 MPa. For the uniaxial yield strengths of A0 and A40, the reported values here are considered as lower-bound (i.e., conservative) estimates because the samples did not produce adequate plastic deformation needed to extract the indentation yield strength corresponding to the 0.2% offset plastic strain (Figure 3a). The relatively small thicknesses of the deposited samples did not permit the application of larger loads without the measurements being affected by the substrate. Prior work has recommended that the contact radius should be less than 1/15th of the sample thickness.[25] The estimated contact radii of the indentation tests did not exceed 400 microns, which is less than 1/15th of the sample

thickness of 7 mm. This suggests that our reported measurements were not significantly affected by the substrate. Further, it is clear that the three samples tested have distinct yield strengths, with A40 showing the highest yield strength value (Table 1).

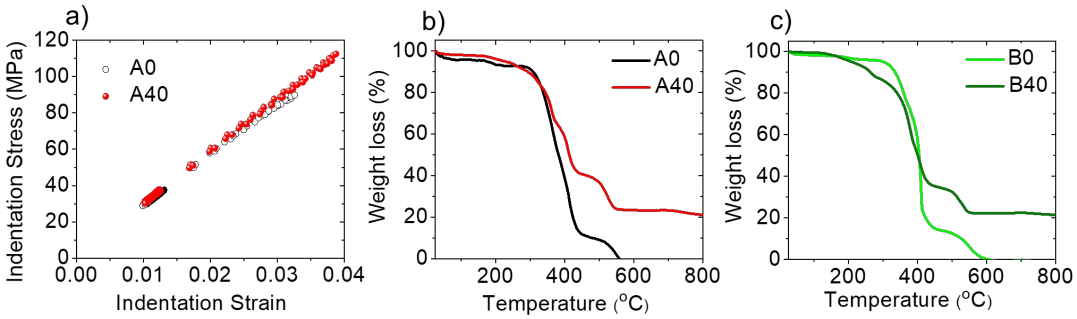

Figure 3. a) Micro indentation analysis of A0 and A40; TGA of b) A0 and A40, and c) B0 and B40.

TGA were done to investigate the thermal stability of the samples A0 and A40 (Figure 3b & 3c). A0 exhibits higher temperature stability (300 °C) when compared to A40 (200 °C). This reduction in decomposition temperature (T_d, 5 % weight loss) is attributed to the early decomposition of carboxylate units in the bismuth compound (Figure 3b). TGA of CMB alone shows decomposition around 226 °C (Figure S4). Similar observations were found for samples B0 and B40, with the latter also showing a decomposition temperature of 200 °C (Figure 3c). DSC analysis of these samples was also done to measure the glass transition temperature (T_g) and decomposition profile (Figure S5). There was no clear observation of a T_g for all the four samples before their decomposition due to the highly cross-linked PVT matrix.

Monte Carlo N-particle (MCNP) modeling

Monte Carlo N-Particle (MCNP) code was used to simulate the response of these plastic scintillators. The current generation of scintillators being developed contain CMB at various compositions, 1 wt.% 4CzIPN, and PVT as the base matrix. A simulation of the various reactions in the material was performed for varying bismuth mass loading. A

main parameter in MCNP is material density, which was calculated for materials at different bismuth loadings using a weighted average approach outlined in Equation 1, where m_i is the mass of each component element and ρ_i is the corresponding density.

$$\rho = \frac{1}{m_{total}} \sum_i \rho_i m_i \qquad (1)$$

This equation yields the results shown in Table S1, which includes a fill factor to quantify a relative amount of bismuth in the material. These density inputs were used to generate reaction type rates as a function of bismuth loading, shown in Figure S6.

It is shown that the low-energy incoherent scattering remains constant across all compositions. However, the coherent scattering (Compton scattering) rate decreases while the photoelectric and fluorescence reactions increase as a function of increasing bismuth loading. The fluorescence reaction rate increases drastically until about 30-35% Bi mass loading and steadily increases thereafter. This result suggests that a viable bismuth loading could be around 30-35%, which will decrease size requirements for detectors. However, quenching below 35% is a current concern being experimentally examined.

A drawback to using MCNP is that it does not capture the specific molecular excitation mechanisms. For example, in large organic molecules, light absorption can change the structure of molecules and allow very rapid electron transit times from one end of the structure to the other, allowing fast energy deposition for those electrons. The specific dynamics and times here need to be modeled in quantum chemistry simulation codes. Future modeling studies will pursue this.

Gamma Spectroscopy

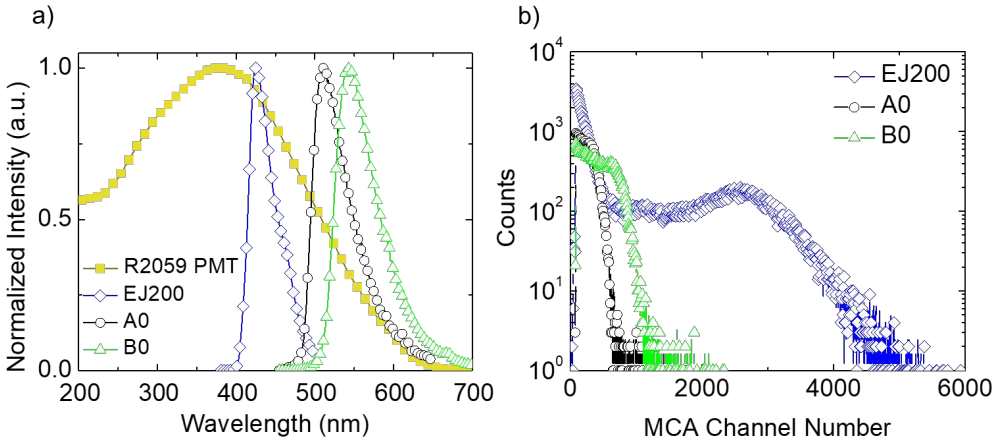

Figure 4. a) Spectral overlap of scintillators EJ-200 (blue), A0 (black), B0 (green) emission spectra and PMT-R2059 QE spectrum (filled squares, yellow) b) ^{137}Cs spectra from EJ-200 (open diamonds, blue), A0 (open circles, black) and B0 (upper triangles, green).

Pulse height spectra for a Cs-137 source for A0, B0 and commercially available EJ-200 were measured under identical conditions. Figure S7 shows the experimental setup. For low-Z nuclei such as those present in these organic scintillators, gamma rays interact with matter via Compton scattering. Nearly all energy deposition events are due to partial energy deposition from the recoiling electron created by the Compton scatter of a gamma ray with an electron bound to one of the scintillator's constituent atoms and molecules. Comparing the Compton edge for 662 KeV gamma-ray, the relative light yields for of A0 and B0 were found to be 0.11 and 0.25, respectively, with EJ-200 scintillation efficiency taken as a reference (light yield of unity, with 10,000 photons /MeV) (Table 3). Figure 4a shows the spectral overlap of emission spectra of scintillators EJ 200, A0 and B0 with quantum efficiency of photomultiplier tube (PMT), PMT-R2059. Even though the overlap integral of tBuCzDBA containing B0 (17.3) is lower compared to that of 4CzIPN loaded A0 scintillator (24.3), B0 scintillators show higher relative light yields than A0 scintillators (0.25 *vs* 0.11) (Table 3). A

photomultiplier tube (PMT), with an enhanced green sensitivity might improve the light yield of these TADF scintillators compared to the blue responsive EJ-200.

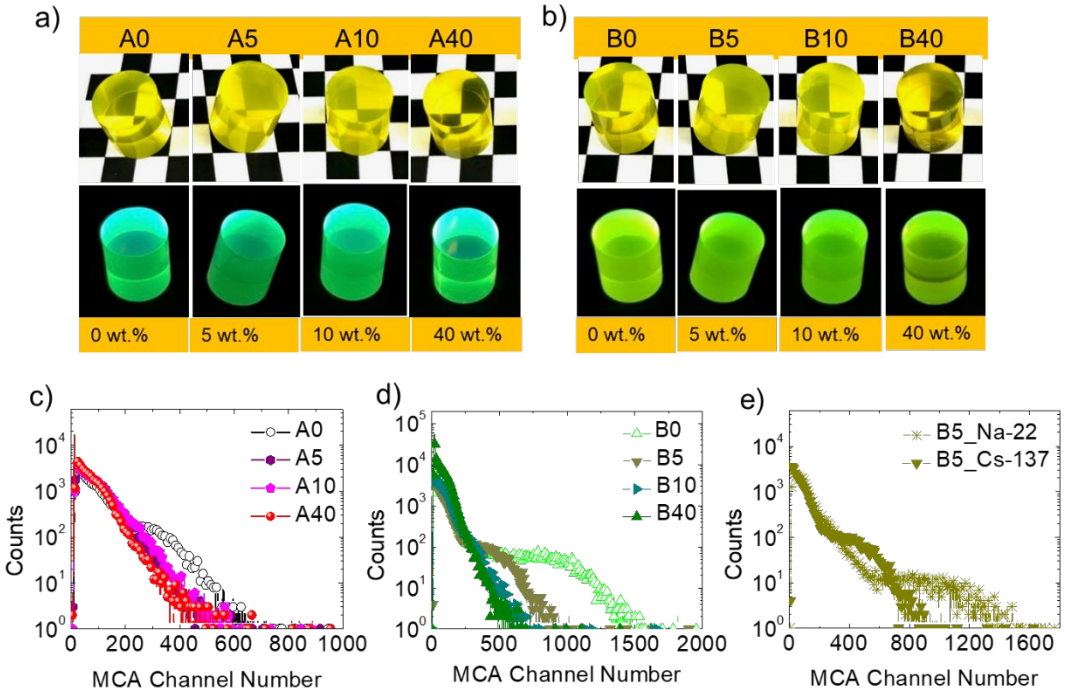

Figure 5. Images of a) 4CzIPN and b) tBuCzDBA loaded scintillators under room light (top) and UV light (365 nm) (bottom) with 0, 5, 10, 40 wt % of CMB) Pulse-height spectra for Cs-137 acquired for all the c) 4CzIPN and (d) tBuCzDBA loaded scintillators and Compton edge for the 662-keV gamma energy is observed in A0 (gray), B0 (light green) and B5 e) Shows Na-22 and Cs-137 measured with B5 (green).

Table 3. Gamma light yields of EJ-200, A0, B0 and B5 scintillators

Scintillator	**Overlap integral (a.u)**	**Volume (cm^3)**	**Relative Light Yield**
EJ-200	37.5	1.84	1
A0	24.3	1.71	0.11
B0	17.3	1.78	0.25
B5	-	1.82	0.14

Also, pulse-height spectra for Cs-137 were acquired for all the 4CzIPN and the tBuCzDBA loaded scintillators with and without bismuth. A Compton edge for the 662-

keV gamma energy is observed in A0, B0 and B5 (Figure 5c & d). Na-22 and Cs-137 were measured with B5, only the Compton edge was observed (Figure 5e). In other bismuth containing samples, the observed signal was too weak to be distinguished from noise. No discernible pattern or underlying structure could be detected. In this case, it appears that the signal was entirely quenched by the bismuth compound, CMB in the scintillator material.

Scintillator with tBuCzDBA dye exhibited higher light yield than 4CzIPN loaded ones. The better light yield for tBuCzDBA loaded scintillator might be due to one or more factors. One possible factor is better outcoupling efficiency. This may be the result of a higher fraction of horizontal emitting dipole orientation for tBuCzDBA at 84% [26] compared to that of 4CzIPN at 73%,[27] or lower internal scattering within the bulk for the sample containing tBuCzDBA. Better energy transfer from the PVT matrix to the tBuCzDBA dye can also be a contributing factor for higher light yield. Even though crosslinking approaches, appear to be useful to improve the mechanical robustness, CMB loading seems to be have an adverse effect on light yield on these TADF loaded scintillators. In order to mitigate this problem, we needed to use high band gap high Z element materials like HfO_2 along with TADF dyes. Our future work will exploit this possibility.

Conclusions

In summary, PVT-based plastic scintillators with TADF dyes, 4CzIPN and tBuCzDBA were developed for radiation detection. Scintillators containing the TADF dye, tBuCzDBA exhibited higher relative light yield than 4CzIPN loaded scintillator (0.25 *Vs* 0.11). A Compton edge for the 662-keV gamma energy was observed in some compositions (A0, B0 and B5). Cross-linking with CMB is found to improve the mechanical properties of the scintillators in terms of uniaxial yield strength values of

66 MPa in scintillators with 40 wt.% loading of CMB. While the use of bismuth-containing compounds can increase gamma–ray matter interaction through the photoelectric effect as guided by MCNP simulations, it also strongly reduces the light yield compared with a commercial plastic scintillator, despite the use of TADF dyes. Alternative ways to overcome this limitation are to replace bismuth compound, CMB with cross-linkable high band gap materials containing Hf.

Author contributions

SA and CF-H and BK conceptualized the project and planned the experiments. SA synthesized CMB, fabricated the scintillators and completed the analysis. HNK and CMT contributed towards the mechanical characterization and SRK supervised the experiments by providing guidance and suggestions. DRK completed the thermal characterization and CWJ supervised that. SM, JCS and NEH contributed toward the radiation detection experiments. KS completed the Monte Carlo N-Particle (MCNP) simulations and MPS supervised that. OM provided suggestions and contributed towards the overlap integral analysis. SA and CF-H wrote the manuscript by the contributions from all the authors.

Conflicts of interest

There are no conflicts to declare.

Acknowledgements

This work was supported in part by the Defense Threat Reduction Agency (DTRA) under grant HDTRA1-18-1-0033 and in part by the Department of Energy/National Nuclear Security Administration under Award DE-NA0003921 through the Consortium for Enabling Technologies and Innovation (ETI). The authors acknowledge Prof. Christopher Jones, Ms. Pavithra Narayanan and Drs. Yadong Zhang and Mathew

Cooper from the Marder Research Group, Georgia Institute of Technology for access to some equipment.

References

1. K. A. Pradeep Kumar, G. A. Shanmugha Sundaram, B. K. Sharma, S. Venkatesh and R. Thiruvengadathan, *Nucl Eng Technol*, 2020, **52**, 2151-2161.
2. S.-i. Okuyama, T. Torii, A. Suzuki, M. Shibuya and N. Miyazaki, *J Nucl Sci Technol*, 2008, **45**, 414-416.
3. T. J. Hajagos, C. Liu, N. J. Cherepy and Q. Pei, *Adv Mater*, 2018, **30**, e1706956.
4. Z. Yang, Z. Mao, Z. Xie, Y. Zhang, S. Liu, J. Zhao, J. Xu, Z. Chi and M. P. Aldred, *Chemical Society Reviews*, 2017, **46**, 915-1016.
5. Y. Li, J.-J. Liang, H.-C. Li, L.-S. Cui, M.-K. Fung, S. Barlow, S. R. Marder, C. Adachi, Z.-Q. Jiang and L.-S. Liao, *J Mater Chem C*, 2018, **6**, 5536-5541.
6. H. Uoyama, K. Goushi, K. Shizu, H. Nomura and C. Adachi, *Nature*, 2012, **492**, 234-238.
7. B. Minaev, G. Baryshnikov and H. Agren, *Phys Chem Chem Phys*, 2014, **16**, 1719-1758.
8. M. W. Cooper, X. Zhang, Y. Zhang, C. Fuentes-Hernandez, S. Barlow, B. Kippelen and S. R. Marder, *Acs Omega*, 2018, **3**, 14918-14923.
9. T. Chen, H. Yu, X. Wen, C. Redding, T. J. Hajagos, H. Zhao, J. P. Hayward, C. Yang and Q. Pei, *Adv Opt Mater*, 2021, **9**, 2001975.
10. T. J. Hajagos, E. Garcia, D. Kishpaugh and Q. Pei, *Nuclear Instruments and Methods in Physics Research Section A: Accelerators, Spectrometers, Detectors and Associated Equipment*, 2019, **940**, 185-198.
11. E. Montbarbon, F. Sguerra, G. H. V. Bertrand, S. Gaillard, J.-L. Renaud, R. B. Pansu and M. Hamel, *Chemphotochem*, 2017, **1**, 451-458.
12. C. Liu, Z. Li, T. J. Hajagos, D. Kishpaugh, D. Y. Chen and Q. B. Pei, *Acs Nano*, 2017, **11**, 6422-6430.
13. N. J. Cherepy, R. D. Sanner, P. R. Beck, E. L. Swanberg, T. M. Tillotson, S. A. Payne and C. R. Hurlbut, *Nucl Instrum Meth A*, 2015, **778**, 126-132.
14. G. H. V. Bertrand, F. Sguerra, C. Dehe-Pittance, F. Carrel, R. Coulon, S. Normand, E. Barat, T. Dautremer, T. Montagu and M. Hamel, *J Mater Chem C*, 2014, **2**, 7304-7312.
15. N. J. Cherepy, S. Hok, S. P. O'Neal, H. P. Martinez, P. R. Beck, R. D. Sanner, O. B. Drury, E. L. Swanberg, S. A. Payne and C. R. Hurlbut, *Hard X-Ray, Gamma-Ray, and Neutron Detector Physics Xx*, 2018, **10762**, 12.
16. S. O'Neal, N. Cherepy, S. Hok and S. Payne, *Ieee T Nucl Sci*, 2020, **67**, 746-

751.

17. B. L. Rupert, N. J. Cherepy, B. W. Sturm, R. D. Sanner and S. A. Payne, *EPL (Europhysics Letters)*, 2012, **97**, 22002.
18. T.-L. Wu, M.-J. Huang, C.-C. Lin, P.-Y. Huang, T.-Y. Chou, R.-W. Chen-Cheng, H.-W. Lin, R.-S. Liu and C.-H. Cheng, *Nat Photonics*, 2018, **12**, 235–240.
19. H. N. Kim, S. Mandal, B. Basu and S. R. Kalidindi, *Integrating Materials and Manufacturing Innovation*, 2019, **8**, 257-272.
20. S. Pathak, J. Shaffer and S. R. Kalidindi, *Scripta Materialia*, 2009, **60**, 439-442.
21. Z. Courtright, N. P. Leclerc, H. N. Kim and S. Kalidindi, *Applied Sciences*, 2021, **11**, 1061.
22. M. T. Abba and S. R. Kalidindi, *Mechanics of Time-Dependent Materials*, 2020, DOI: 10.1007/s11043-020-09472-y.
23. J. S. Weaver, A. Khosravani, A. Castillo and S. R. Kalidindi, *Integrating Materials and Manufacturing Innovation*, 2016, **5**, 192-211.
24. D. K. Patel and S. R. Kalidindi, *Acta Materialia*, 2016, **112**, 295-302.
25. S. Mohan, N. Millan-Espitia, M. Yao, N. V. Steenberge and S. R. Kalidindi, *Experimental Mechanics*, 2021, **61**, 641-652.
26. T.-L. Wu, M.-J. Huang, C.-C. Lin, P.-Y. Huang, T.-Y. Chou, R.-W. Chen-Cheng, H.-W. Lin, R.-S. Liu and C.-H. Cheng, *Nature Photonics*, 2018, **12**, 235-240.
27. J. W. Sun, J.-H. Lee, C.-K. Moon, K.-H. Kim, H. Shin and J.-J. Kim, *Adv Mater*, 2014, **26**, 5684-5688.